Unsteady Viscous Flow on Oscillating Airfoils

W. J. McCroskey*
U.S. Army Air Mobility R & D Laboratory, Moffett Field, Calif.
AND
J. J. Philippe†
Office National d'Etudes et de Recherches Aérospatiales, Châtillon, France

Incompressible laminar and turbulent flows over flat plates and airfoils have been investigated numerically and experimentally in unsteady flow conditions. Important differences were found between laminar and turbulent flat plate flows over a wide range of oscillation frequencies. Also, the importance of unsteady effects on laminar boundary layers was found to diminish rapidly with increasing longitudinal pressure gradients, whereas turbulent separation on airfoils was significantly affected by oscillatory motion when the incidence approached the stall angle. The calculated hysteresis in turbulent separation followed in a qualitative sense the well-known trends of dynamic stall delay and reattachment. However, the numerical analysis failed to indicate some of the important features of dynamic stall observed in the present experiment and in previous studies.

Nomenclature

A = amplitude of fluctuating free stream velocity
C_p = pressure coefficient, $(p-p_\infty)/\frac{1}{2}\rho U_\infty{}^2$
ΔC_p = differential pressure coefficient, $C_{p_{\text{upper}}} - C_{p_{\text{lower}}}$
C_f = skin friction coefficient, $\tau_w/\frac{1}{2}\rho U_\infty{}^2$
C_M = pitching moment coefficient
C_N = normal force coefficient
c = airfoil chord, m
F, G = real and imaginary parts of the Theodorsen function
F^*, G^* = real and imaginary modified Theodorsen functions for velocity
f' = nondimensional boundary layer velocity, u/U_e
H = shape factor, δ^*/θ
k = reduced frequency, $\omega c/2U_\infty$
l = nondimensional turbulent viscosity, $(\varepsilon+\nu)/\nu$
l_1 = length of the laminar shear layer, m
l_2 = length of the turbulent mixing and reattachment region, m
M = Mach number
n = exponent in turbulent velocity profile, $u/U_e = (y/\delta)^{1/n}$
Re = Reynolds number based on U_∞ and c
Re_x = Reynolds number based on U_o and x
Re_θ = Reynolds number based on U_e and θ
r_o = leading edge radius, m
t = time, sec
U_o = average stream velocity, m/sec
U_∞ = freestream velocity, m/sec
U_e = velocity at the outer edge of the boundary layer, m/sec
V_t, V_c, V_a = thickness, camber, and angle-of-attack components of U_e on a static airfoil
u = streamwise velocity in the boundary layer, m/sec
v = vertical velocity in the boundary layer, m/sec
X = chordwise distance, normalized by c
x = surface distance from the leading edge and streamwise boundary layer coordinate, m
x_o = location of the stagnation point, m
Y = airfoil coordinate, normalized by c
y = normal boundary layer coordinate, m
α = angle of attack, $\alpha = \alpha_0 + \alpha_1 \sin \omega t$, deg
β_x = longitudinal pressure gradient parameter, $(\xi/U_e)(\partial U_e/\partial \xi)$
β_t = unsteady pressure gradient parameter, $(\omega\xi/U_e{}^2)(\partial U_e/\partial \tau)$
δ = boundary-layer thickness
δ^* = boundary-layer displacement thickness
ε = eddy viscosity
η = transformed vertical boundary-layer coordinate
θ = momentum thickness
ν = kinematic viscosity
ξ = transformed boundary-layer coordinate, $x-x_o$
ρ = density
σ = Crabtree pressure recovery factor for bubble bursting
τ = dimensionless time in Eqs. (3) and (4), shear stress elsewhere
ϕ = phase angle relative to the quasi-steady value, deg
ω = frequency of oscillation, rad/sec

Presented as Paper 74-182 at the AIAA 12th Aerospace Sciences Meeting, Washington, D.C., January 30–February 1, 1974; submitted February 22, 1974; revision received July 29, 1974. Research conducted under the provisions of the Memorandum of Understanding between France and the United States for a Cooperative Research Project in Helicopter Dynamics.

Index categories: Boundary Layers and Convective Heat Transfer—Turbulent; Nonsteady Aerodynamics; Rotary Wing Aerodynamics.

* Research Scientist, Ames Directorate. Associate Fellow AIAA.
† Research Scientist.

I. Introduction

THE ability to predict the aerodynamic behavior of many devices that employ unsteady lifting surfaces is often comprised by our inadequate theoretical understanding of the viscous effects involved. Dynamic stall, in particular, produces transient variations in forces and moments that are fundamentally different from their steady-state counterparts, and the physical mechanisms involved are not well understood. The present investigation was motivated by two main questions relative to this phenomenon: 1) how far can the classical concepts and analyses of thin, non-interacting boundary layers be pushed, and 2) what could be inferred about dynamic stall from such an exercise?

This paper describes a combined numerical analysis and experimental study of detailed unsteady laminar and turbulent boundary-layer characteristics, continuing to build upon the preliminary results for oscillating airfoils that were reported in Refs. 1–3. Martin et al.[1] combined flow visualization and pressure measurements to demonstrate that an important element of dynamic stall is the formation and shedding of a powerful vortex-like disturbance from the leading edge of the airfoil, as indicated in Fig. 1. This vortex produced the types of transient pressure distributions shown in Fig. 2. The qualitative features of this phenomenon resemble the vortex-shedding model of Ham and Garelick.[4] These investigators, and more recently Philippe and Sagner,[2] modeled this phenomenon with potential vortices, and were able to produce the general types of pressure distributions that had been observed. However, the incidence at which the theoretical vortex shedding was initiated had to be assumed arbitrarily, or taken from experiments. Of course, this limitation reflects the need to examine this viscous flow in more detail.

Although dynamic stall is recognized to be a strong viscous-inviscid interaction phenomenon, and Crimi and Reeves[5] have recently made an ambitious attempt to treat it as such, a full

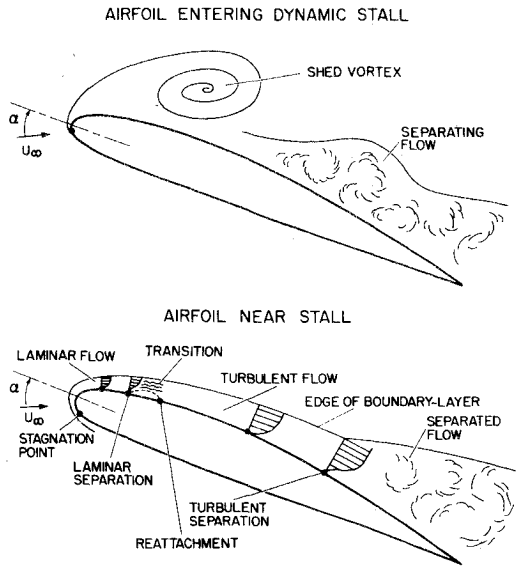

Fig. 1 Flowfield around airfoils at high incidence.

and correct treatment of the problem seems beyond the present state of the art in fluid mechanics. There appears to be a great deal still to be learned about unsteady viscous flows within the more tractable framework of classical thin boundary-layer theory; and as mentioned earlier, this is the approach we have adopted in the theoretical analysis that follows. It should be emphasized that we are more interested in the relative changes that occur when unsteady effects are included, rather than in the absolute values of the boundary-layer characteristics in either the steady or the unsteady case.

II. Description of Methods

Theoretical Model

The lower half of Fig. 1 indicates the theoretical model that was chosen for the boundary-layer analysis on oscillating airfoils. The stagnation point location and potential flow velocity distribution required for the boundary-layer calculations were obtained from the unsteady solution formulas of McCroskey,[6] which split U_e into thickness, camber, and angle-of-attack components as follows:

$$U_e = V_t \pm V_c \pm V_a \alpha T \tag{1}$$

where the signs refer to the upper and lower surfaces of the airfoil, respectively, and for sinusoidal oscillations, $\alpha = \alpha_0 + \alpha_1 \sin \omega t$, in pitch about the quarter-chord,

$$\alpha T = \alpha_0 + \alpha_1(F^* - kG^*)\sin \omega t + \alpha_1(G^* + kF^* + 2k[X - 1/4])\cos \omega t \tag{2}$$

The airfoil functions $V_t(X)$, $V_c(X)$, and $V_a(X)$ were calculated from steady airfoil theory using a method of singularities, and the unsteady velocity functions $F^*(X,k)$ and $G^*(X,k)$ are modified forms of the thin airfoil Theodorson solution,[7] $F(k)+iG(k)$. This approach has been shown in Ref. 6 to give simple and accurate results in the absence of stall.

Figure 1 indicates a thin laminar boundary-layer flow near the leading edge, followed by transition to turbulence by the mechanism of a short separation bubble. More will be said on this point later. Transition by virtue of the growth of laminar instabilities was also considered, within the framework of the empirical methods of Bennett[8,9] and Michel.[9,10] This type of instability-triggered transition was predicted to occur only at high Reynolds numbers and low angles of attack, well below the stall angle.

The turbulent boundary-layer flow was modeled by incorporating the eddy viscosity formulation of Cebeci et al.[11] into the time-dependent mean momentum equation, derived and

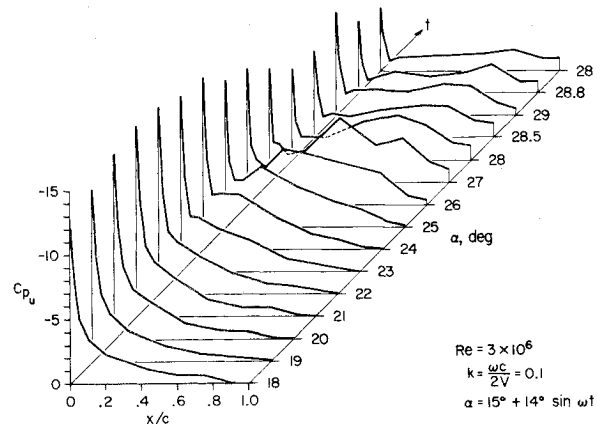

Fig. 2 Time history of the effect of dynamic stall on the pressure distribution on the upper surface of an airfoil.[1]

discussed by Shamroth and McDonald.[12] The unsteady term $\partial U_e/\partial t$ was incorporated into Cebeci's pressure gradient correction to the sublayer damping length, but the various empirical constants in his formulation were not modified for unsteady effects. Therefore, the physics of the local turbulence field was effectively assumed to be quasi-steady.

With regard to the question of the separation points indicated in Fig. 1 and subsequent figures, it should be mentioned that Sears and Telionis[13] have warned that "separation" cannot always be interpreted as the point of vanishing wall shear, or flow reversal, in unsteady flows. However, the correct analytical definition of unsteady separation remains an open question, especially in cases of turbulent flow. As discussed by Shamroth and McDonald[12] it would seem that within the thin boundary-layer framework that we have adopted, the trends in the locus of $C_f = 0$ would follow "separation" trends closely, especially in airfoil-type flows with large adverse pressure gradients. Therefore, no attempt has been made in this investigation to distinguish between the two. Admittedly, future developments may call this decision into question.

Remarks on Separation Bubbles

Since the theoretical model excludes viscous-inviscid interaction, the boundary-layer calculations give no direct indication of either static or dynamic stall, with the possible exception of predicting that the separation bubble near the leading edge will fail to reattach, that is, that it will "burst." The sketches in Fig. 3 indicate the commonly-assumed features of the leading edge bubble, which starts at the point of laminar separation. The bubble perturbs the inviscid velocity distribution only between the separation and reattachment points S and R, respectively, and in the general manner shown. At distance l_1 downstream of

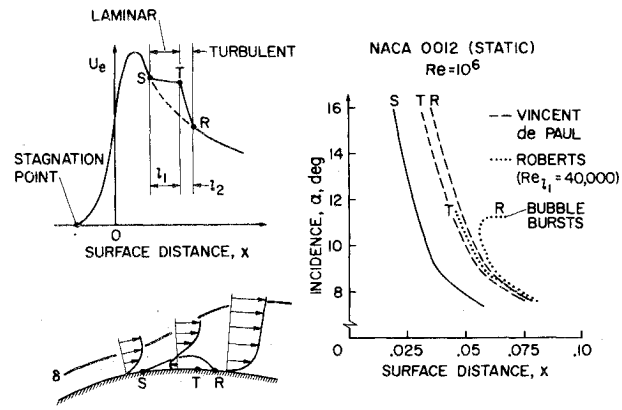

Fig. 3 Leading edge separation bubble on an airfoil at high incidence. S, laminar separation; T, transition; R, turbulent reattachment.

laminar separation, the free shear layer changes abruptly at T to a turbulent one of length l_2. The locations of S, T, and R depend upon the airfoil shape, pitch axis location, angle of attack, and pitch rate. The position of laminar separation is theoretically independent of Reynolds number, but the locations of T and R are not.

If the flow is able to overcome the pressure rise across the bubble necessary to decrease U_e from the value at S to the theoretical value that would exist at R in the absence of the bubble, the turbulent free shear layer reattaches at R and becomes an ordinary turbulent boundary layer downstream. Otherwise, the bubble is said to burst, and this precipitates what is commonly called leading edge stall. Therefore, for this type of stall, we should be able to predict the stall angle using an analysis of bubble bursting.

The most recent bubble analyses that have come to the authors' attention are those of Crimi and Reeves,[5] Horton,[14] Vincent de Paul,[15] Lang[16], and Roberts.[17] Each analysis gives the variations in boundary layer characteristics across the bubble, the lengths l_1 and l_2, and the maximum permissible velocity drop $\Delta U_e = U_{e_S} - U_{e_R}$, that is, the criterion for bubble bursting. While each method has been compared favorably with one or more experiments, unfortunately the results vary considerably when the same case is considered for all. For example, Fig. 3 shows the predictions of two methods for the variation with incidence of the points T and R on a static NACA 0012 airfoil at a constant Reynolds number of 10^6. In addition to the differences in the locations of T and R, Roberts' method predicts the bubble to burst at $\alpha \approx 11.2°$, whereas Vincent de Paul predicts no bursting for angles as high as 20°.

In hopes that the bubble analyses would shed some light on both the static and dynamic stall characteristics of the NACA 0012 airfoil, the bubble-bursting angles were calculated by each method as a function of Reynolds number. The static results are shown in Fig. 4, in comparison with the experimental stall angles from a number of sources[1,18-23] and unpublished data that were obtained at the U.S. Army AMRDL during the course of the experiment described in Ref. 6. According to the stall classification criterion of Gault,[24] the NACA 0012 airfoil should exhibit either leading edge stall or combined leading edge and trailing edge stall over most of the Reynolds number range displayed, and bubble-bursting is commonly believed to play an important role in this case. Unfortunately, there does not seem to be much correlation between the predicted bursting angles and the measured stall angles. For this reason, the bursting predictions were not pursued further to any great extent. However, the results of these analyses were incorporated into the main boundary-layer program, described in the next section, to provide starting conditions for the turbulent flow at higher Reynolds numbers.

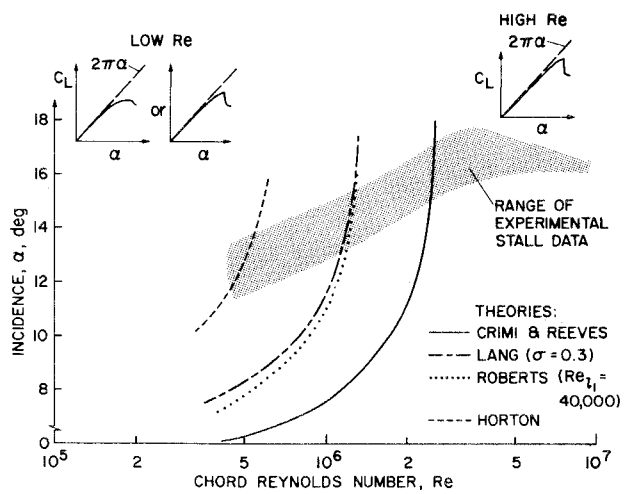

Fig. 4 Predictions of bubble-bursting angles on a static NACA 0012 airfoil.

Numerical Method

The basic numerical method used to integrate the unsteady boundary-layer equations was the implicit finite difference scheme of Dwyer.[25,26] The transformation $\xi = x - x_o$, $\eta = (U_e/2\xi\nu)^{1/2}y$, $\tau = \omega t$ was applied to the unsteady boundary-layer equations, giving the following equations for continuity and momentum, respectively:

$$\xi\frac{\partial f'}{\partial \xi} + \frac{\partial V}{\partial \eta} - \frac{1}{2}[\beta_t - (\beta_x + 1)f'] = 0 \tag{3}$$

$$\frac{\omega\xi}{U_e}\frac{\partial f'}{\partial \tau} + \xi f'\frac{\partial f'}{\partial \xi} + V\frac{\partial f'}{\partial \eta} + \beta_t(f' - 1) + \beta_x(f'^2 - 1) - \frac{1}{2}\frac{\partial}{\partial \eta}\left(l\frac{\partial f'}{\partial \eta}\right) = 0 \tag{4}$$

where

$$f'(\xi, \eta, \tau) = \partial f/\partial \eta = u/U_e$$

$$V = (U_e\xi/2\nu)^{1/2}(v/U_e) + \eta/2[\beta_t + (\beta_x - 1)f']$$

$$\beta_x = (\xi/U_e)(\partial U_e/\partial \xi); \quad \beta_t = (\omega\xi/U_e^2)(\partial U_e/\partial \tau)$$

$$l = (\varepsilon + \nu)/\nu$$

The shear stress in the physical domain is given by $\rho(\varepsilon + \nu)(\partial u/\partial y)$.

Central differences at each unknown grid station were used to evaluate the η-derivatives, and backward differences were used for the τ- and ξ-derivatives. The Crank-Nicolson method[27] of differencing was used in the laminar case with $l = 1$, but this was changed to a fully implicit scheme in the turbulent case with variable l, where iterations on the transport properties were required at each x-station. In either case, the resulting set of simultaneous difference equations have a tridiagonal matrix form and are rapidly solved by the Thomas algorithm.[27]

To start the computations, "initial" conditions in both ξ and τ had to be specified. By virtue of the transformation employed, laminar conditions at the stagnation point could be obtained simply by taking the limit $\xi \to 0$ in Eqs. (3) and (4). The initial conditions in τ were approximated by starting the calculations at a time in the cycle when $\beta_t \approx 0$ and suppressing the term $(\omega\xi/U_e)(\partial f'/\partial \tau)$ in Eq. (4). The small error so introduced damped out during the course of the first cycle of oscillation.

The problem of specifying the starting conditions at the first turbulent station, which was always downstream of $\xi = 0$, proved to be more troublesome. Following Dwyer et al.,[26] the technique employed was to approximate the velocity profile by a power law variation in the "wall" and "wake" regions and by a linear variation in the viscous sublayer. This required that three parameters be specified: the boundary-layer thickness, the local skin friction coefficient, and the power law exponent. However, in some cases it was quite difficult to choose these parameters accurately, and the resultant errors often propagated many x-stations downstream before dying out. This problem was finally resolved to a reasonable extent by iterating several times on the initial f' and V profiles before marching downstream to the first new turbulent station, and by carefully tailoring the choice of the three free parameters to the specific problem at hand. Several examples are cited in Sec. III.

Typical "production" calculations entailed $1\frac{3}{4}$ cycles of oscillation, with 18 time steps per cycle. Fourteen x-stations were normally used for flat plate calculations, and 30 for airfoils. Calculation times on an IBM 360/67 computer varied from about one minute for the laminar flat plate to about $7\frac{1}{2}$ min for the longest turbulent airfoil case.

Experiments

The literature abounds with experiments on oscillating airfoils, but in the majority of cases, measurements have not been made of the quantities that can be calculated readily from boundary-layer theory. Therefore, the U.S. Army AMRDL and the ONERA have undertaken several projects that are intended to provide guidance and insight for the theoretical studies and to evaluate some of the calculations of boundary-layer characteristics.

The airfoils chosen for these studies are the NACA 0012 in the United States and a derivative profile with leading edge

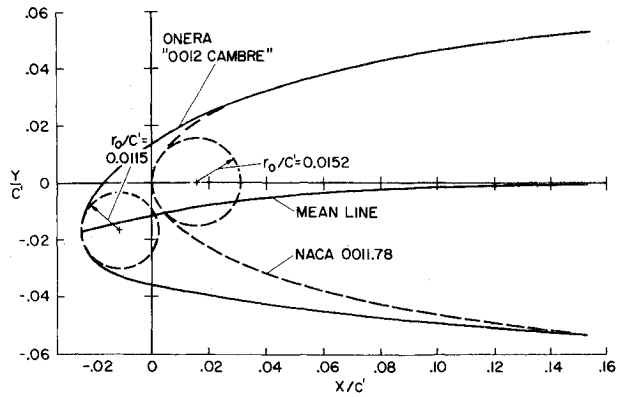

Fig. 5 Leading edge extension of the ONERA cambered airfoil. Actual chord = 1.025 c'.

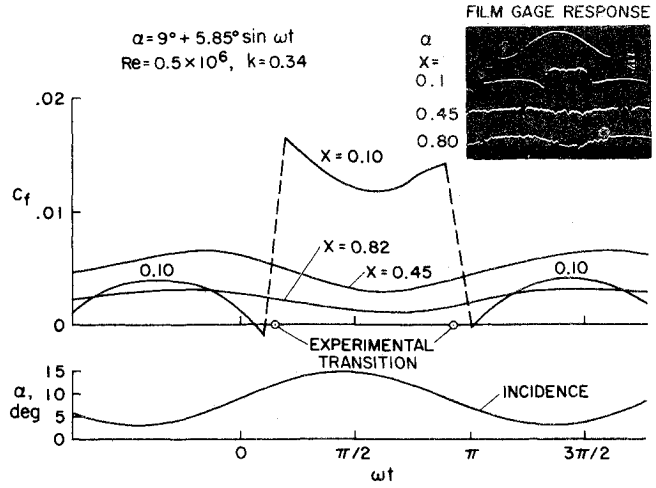

Fig. 7 Variation of theoretical and experimental skin frction through a cycle of oscillation; ONERA cambered airfoil.

camber, known as the "0012 à Extension Cambrée," in France. Preliminary results appear in Refs. 1–3. Figure 5 indicates how the ONERA profile was generated by adding a 2½% leading edge extension to an 11.78% thick profile of the symmetrical NACA 00XX Series. This extension lowers the leading edge velocity peak, as shown in Fig. 6, and increases the maximum lift capability, without significantly affecting the pitching moment characteristics. An interesting aspect of the ONERA airfoil is the irregular variation in U_e near the leading edge. This is somewhat similar to the characteristics of the NACA 22012 and 23012 airfoils, which have generally similar mean lines, although the quantitive behavior of the camber function, V_c, of these profiles is different.

The measurements reported herein were obtained on two ONERA 0012 Cambré models. Each oscillated in pitch about the quarter-chord at a fixed amplitude of $\pm 6°$; the mean angle of attack was varied from 0° to 15°. The smaller model (0.27 m chord) was instrumented with surface-mounted heated film skin friction gages of the type described in Refs. 2 and 28, and with hot wire anemometers near the outer edge of the boundary layer. It was tested at $M \approx 0.07$, $Re \approx 0.5 \times 10^6$ in the ONERA 1 m diam Wind Tunnel S2L at Chalais-Meudon. The larger model (0.41 m chord) was instrumented with four skin friction gages and ten miniature pressure transducers, and it was tested at $M \approx 0.2$, $Re \approx 1.9 \times 10^6$ in Wind Tunnel S10-Centre d'Essais Aéronautique de Toulouse. Data were also obtained at higher Mach numbers in the CEAT facility; these will be reported in a subsequent ONERA publication.

The heated film skin friction gages were used to help determine the state of the boundary layer, e.g., laminar, transitional, turbulent, or separated, at various chordwise stations as the model incidence varied. Representative oscilloscope signals for laminar and turbulent flows can be seen in the inset of Fig. 7. As discussed in Ref. 28, the hot film gage signal is approximately proportional to a fractional power of the instantaneous wall shear. Therefore, the abrupt rise and fall of the signal at $X = 0.1$ is interpreted as the passage of a separation bubble and the associated abrupt transition back and forth over the gage as α increases and decreases. We shall return to the discussion of the measured and calculated results in this figure in Sec. III.

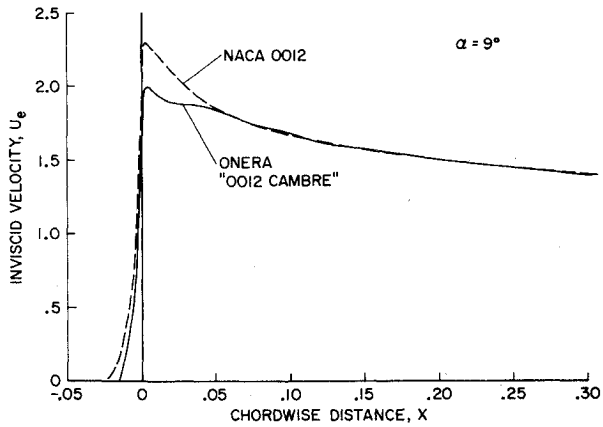

Fig. 6 Representative velocity distributions on the NACA and ONERA airfoils.

III. Results and Discussion

Flat Plate in an Oscillating Stream

As a prelude to the study of complex unsteady viscous flows on airfoils, the relative simplicity of the flat plate boundary-layer makes this problem attractive for exploring certain basic unsteady phenomena. Many studies of the case $U_e = U_o(1 + A \sin \omega t)$, including, for example, the classic analysis of Lighthill[29] and the experiments of Hill and Stenning[30] and Karlsson,[31] have shown that the magnitude of the boundary-layer velocity profiles and their phase with respect to U_e are strongly influenced by unsteady effects. At low frequencies, including the range of interest for the airfoil cases to be considered later, unsteady effects are approximately proportional to the local reduced frequency, $\omega x/U_o$, and the Lighthill analysis[29] gives the relative amplitude of the wall shear fluctuation, $\tau_1/\tau_0 = \frac{1}{2}[1 + 2.89(\omega x/U_o)^2]^{1/2}$, and the phase with respect to U_e is $\phi = \tan^{-1}(1.70\omega x/U_o)$. In the high-frequency limit, Lighthill showed that unsteady effects are confined to a thin shear wave layer near the wall, whose thickness is of order $(\nu/\omega)^{1/2}$. In this case, $\tau_1/\tau_0 = 3.01(\omega x/U_o)^{1/2}$ and the wall shear leads U_e by a phase angle $\phi = \pi/4$.

Figure 8 shows the calculated results for wall shear for the laminar flat plate problem, in comparison with the results of Lighthill. The laminar calculations of phase angle smoothly bridge the gap between the low and high-frequency approximations, as would be expected, and the results are independent of Reynolds number.

The high-frequency turbulent results‡ are surprisingly different. In Fig. 8, the phase angle of τ_w is seen to be Reynolds number dependent, and more significantly, there is no evidence of a counterpart to the Lighthill "shear wave" solution that exists at the bottom of a high-frequency laminar boundary layer. The magnitude of the wall shear hardly changes with increasing frequency, and the phase remains close to that of U_e. There-

‡ The present calculations were performed for a flat plate with $c = 3$ m. Transition was assumed at $x/c = 0.1$, and the initial turbulent profiles were calculated using $n = 6$, $\theta = 0.036x\,Re_x^{-1/5}$, $\delta/\theta = (2+n)(1+n)/n$ and $C_f = 0.0256\,Re_\theta^{-1/4}$, based on the formulas in Ref. 32.

fore, on the basis of τ_w alone, it would seem that the turbulent flow is approximately quasi-steady over a wide frequency range.

However, this conclusion is quickly dispelled by the results shown in Fig. 9. The unsteady turbulent displacement thickness shows even larger variations with reduced frequency than the laminar results. This means that while the flow at the surface seems nearly quasi-steady, the flow in the interior of the boundary layer is strongly affected by unsteady effects.

Also shown in Fig. 9 are recent turbulent calculations by Singleton and Nash[33] which were based on a turbulent kinetic energy formulation, and results derived from the measurements of Karlsson.[31] With regard to the latter, it should be mentioned that Karlsson's measurements were made in a tripped boundary layer on the wall of a wind tunnel with a long test section, and for the purposes at hand, this condition was somewhat arbitrarily assumed equivalent to a flat plate of 3 m in length. Also, the scatter in the data made a precise determination of δ^* impossible, hence the possibility of the sorts of uncertainty indicated in the figure. Nevertheless, certain clear trends in the results are readily distinguishable.

All of the calculations agree fairly well with the data intermediate frequency range $1 \lesssim \omega x/U_o \lesssim 2$, where the unsteady effects are quite large. However, in the range $4 \lesssim \omega x/U_o \lesssim 6$, both the data and Singleton and Nash's turbulent kinetic energy calculations show a definite trend to negative values of ϕ_{δ^*}. This indicates that more of the boundary layer is lagging the quasi-steady behavior than is leading it, but this phenomenon is not captured by the present eddy viscosity calculations. As ω increases, the data clearly show a return to positive $\phi_{\delta}{}^*$ for $\omega x/U_o \gtrsim 8$, followed by a decay to zero as $\omega x/U_o \to \infty$, and this trend is not captured by the turbulent kinetic energy results.

A final point concerns the nonlinear effects of large amplitudes of oscillation. In Lighthill's analysis, the amplitude of the laminar wall shear increases monotonically with both the amplitude of U_e and with reduced frequency. Therefore, flow reversal, i.e., $\tau_w < 0$, is predicted for sufficiently large values of the quantity

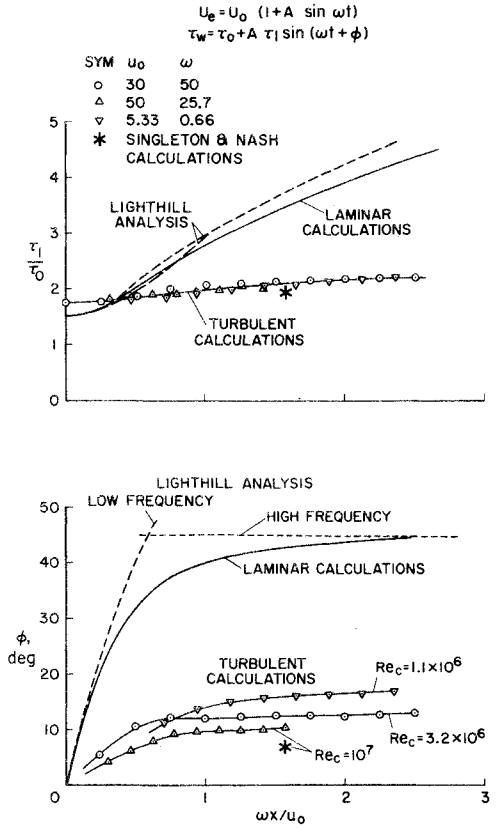

Fig. 8 Amplitude and phase of the skin friction fluctuations on a flat plate in an oscillating stream; laminar and turbulent calculations; $A = 0.125$.

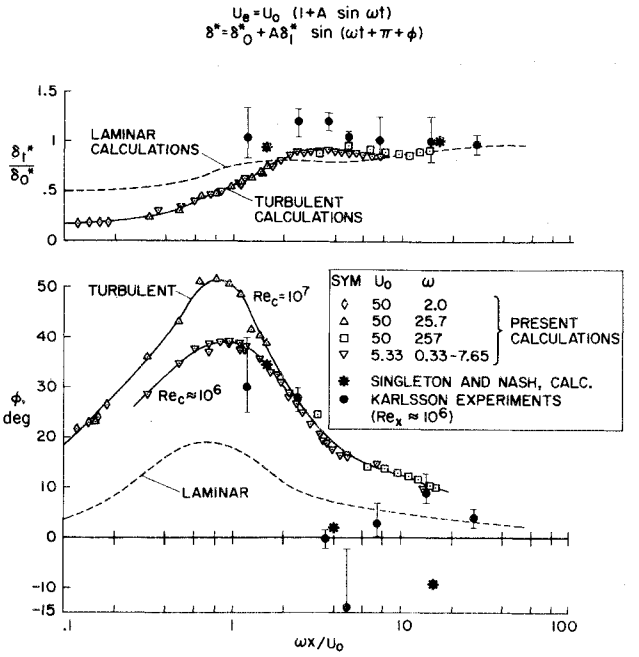

Fig. 9 Amplitude and phase of the boundary layer displacement thickness fluctuations on a flat plate in an oscillating stream; $A = 0.125$.

$A(\omega x/U_o)$. Nonlinearities in the full equations tend to suppress this trend toward flow reversal, but additional calculations showed the flow reversal condition to be attainable in the laminar case. In the turbulent case, the smaller values of τ_1 shown in Fig. 8 combine with the nonlinearities in the full equations to suppress the tendency toward flow reversal even more. To the best of the authors' knowledge, the existence of this type of flow reversal that is induced solely by unsteady effects remains to be demonstrated experimentally in the flat plate case.

The main features of the unsteady flat plate case, then, can be summarized as follows: In the low frequency limit, the phase angles of both laminar and turbulent τ_w and δ^* approach zero linearly as $\omega x/U_o \to 0$. The magnitudes of τ_1 and $\delta_1{}^*$ reflect the parabolic growth of the mean laminar boundary layer and the approximate $\frac{4}{5}$-power growth of the mean turbulent boundary layer. In the high frequency limit, the "shear wave" solution dominates the laminar boundary near the wall, with ϕ_τ approaching 45° and τ_1 apparently growing without bound. Not so in the turbulent case, however, as ϕ_τ remains small and τ_1/τ_0 remains of order 2. At very high reduced frequencies, the flow in the middle of the boundary layer is locked in phase with U_e, whether laminar or turbulent, and $\delta_1{}^* \to 1$, $\phi_\delta{}^* \to 0$. The laminar boundary layer makes a smooth transition from one regime to the other when $\omega x/U_o$ is of order 1. The magnitude and phase of turbulent wall shear remain close to their quasi-steady values in this mid-frequency range, but the phase angle of the displacement thickness attains very large positive values, i.e., δ^* leads the quasi-steady solution by a significant amount.

As the reduced frequency is successively increased, the experimental value of $\phi_\delta{}^*$ goes negative (lagging the quasi-steady solution), returns positive, and finally approaches zero as $\omega x/U_o \to \infty$. Neither the eddy viscosity nor the turbulent kinetic energy analysis fully captures this very high frequency behavior, although both methods appear to be adequate for the problems of practical interest at lower frequency.

Airfoils Oscillating in Pitch

We turn our attention now to the more difficult problem of viscous flow with pressure gradients, on oscillating airfoils with $\alpha = \alpha_0 + \alpha_1 \sin \omega t$. In view of the complexity of this problem, and all the qualifications and limitations discussed in Secs. I and II, it seems appropriate to first look briefly at the static case, and

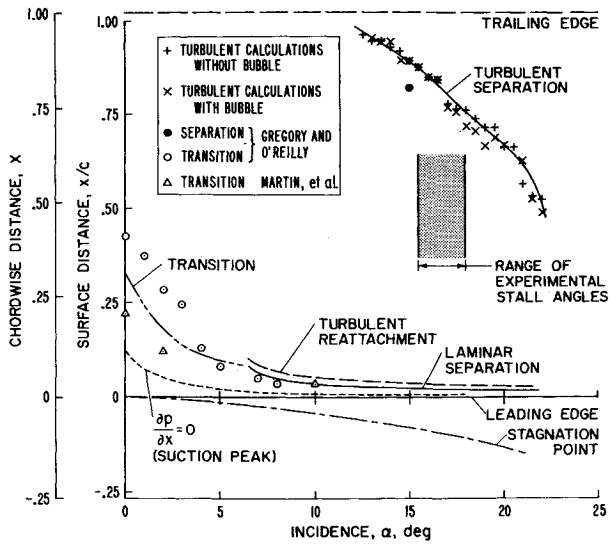

Fig. 10 Static boundary layer characteristics on an NACA 0012 airfoil at $Re = 3 \times 10^6$.

then use this as a frame of reference for the dynamic cases that will follow.

Static airfoil

Figure 10 shows the calculated boundary-layer characteristics on an NACA 0012 airfoil at $Re = 3 \times 10^6$, along with relevant data at approximately the same Reynolds numbers from Refs. 1 and 18. The laminar flow starts at the stagnation point, which moves rearward along the lower surface of the airfoil as α increases, and the laminar condition always persists beyond the suction peak, i.e., beyond the locus of $dp/dx = 0$. At low incidence, transition to turbulence occurs by the mechanism of laminar instability, and the calculated point of transition is in reasonable agreement with experiments. For $\alpha \gtrsim 6.5°$, this type of transition is preceded by laminar separation. Then the separation bubble comes into the picture, as discussed in Sec. II.

The bubble characteristics for all the cases to be discussed in this section were calculated using Lang's formulas[16] for l_1 and l_2 and Horton's formula[14] for θ_R. The turbulent calculations labeled "with bubble" in the figure were started at x_R in the manner described in Sec. II, with the following values: $n = 6 + \beta_x$, where $\beta_x = (\xi_R/U_R)(\partial U_R/\partial \xi)$; $H_R = 2.5$; $\delta_R = (1+n)\theta_R H_R$, and $C_f = 0.0256\, Re_{\theta_R}{}^{-1/4}$. The turbulent calculations labeled "no bubble" were started at the point of laminar separation, x_S, using the same relations for n, H, and δ, except that β_x, θ, and Re_θ were evaluated at x_S instead of x_R. There does not seem to be any systematic difference in the results near the trailing edge for the two sets of calculations shown in Fig. 10, nor in the results that follow. The measured separation point[18] at $\alpha = 15°$ is in fair agreement with the calculated point of $C_f = 0$ at that angle.

Since the bubble was not predicted to burst at this Reynolds number and since no viscous-inviscid interaction is allowed in the theoretical model employed, the calculations could continue past the experimental stall angle. The results in Fig. 10 show a smooth variation in the calculated locus of $C_f = 0$, which would seem to imply the gradual type of stall that would normally be classified as trailing edge stall. However, the measured stall[1,18-23] in this Reynolds number regime was reported to be abrupt, as indicated in the right-hand inset of Fig. 4. This would seem to suggest leading edge stall precipitated by bubble bursting, were it not for the fact that Gregory and O'Reilly[18] reported that the general stall characteristics at $Re = 2.9 \times 10^6$ hardly changed when the bubble disappeared prior to stall, either of its own volition or due to surface roughness. If, as their results suggest, the bubble truly plays only a passive role in the static stall process, then the abrupt flow breakdown must originate somewhere in the turbulent boundary layer. One such possibility is a phenomenon proposed by Wallis[34]; namely a sudden "reseparation" of the flow shortly downstream of the bubble. No such behavior is apparent in the present calculations, but due to the lack of definitive experimental evidence on the NACA 0012 airfoil, it is not clear whether this is a major deficiency.

Oscillating NACA 0012

Figure 11 shows the calculated results for the NACA 0012 profile oscillating in pitch about the quarter-chord with an amplitude of $\pm 6°$, at $Re = 3 \times 10^6$ and $k = 0.24$. Two cases are shown, with mean incidences of 6° and 15°. The curves labeled "quasi-steady" in Fig. 11 were generated by utilizing the unsteady potential flow solution for U_e, but suppressing all unsteady terms in the boundary-layer calculations. Comparing the solid and dashed curves gives an approximate idea of the relative importance of unsteady viscous and unsteady inviscid effects. The various boundary-layer events shown in the figure are delayed relative to the static case when the incidence is increasing; i.e., they occur farther from the leading edge for a given value of α, or at a larger incidence for a given value of x/c. Conversely, the same events occur sooner when α is decreasing. This hysteresis follows the general trends of the aerodynamic forces and moments on oscillating airfoils that experience dynamic stall.

For the case $\alpha_0 = 6°$ and $Re = 3 \times 10^6$, transition by instability is predicted for the lower part of the cycle, where the incidence is lower and the pressure gradients are weaker. On the other hand, turbulence follows laminar separation and a bubble occurs during the upper part, at higher incidence. There is little significant effect of the hysteresis in the locus of transition on the subsequent turbulent boundary-layer development downstream. The curve labeled "$C_f = 0$ (laminar without transition)" shows what would happen at very low Reynolds numbers. In this low-incidence case, the unsteady pressure gradient due to $\partial U_e/\partial t$ is comparable in importance to the spatial term, $U_e(\partial U_e/\partial x)$, over much of the cycle. This produces a large hysteresis loop, which is further enhanced by the inclusion of unsteady viscous effects. However, at the large angles associated with the $15° \pm 6°$ case, the spatial pressure gradient term almost completely dominates the laminar separation characteristics, and the bubble characteristics as well at this Reynolds number. Consequently, very little laminar hysteresis is observed in this case. Therefore, the large differences between static and dynamic stall that have been observed[1] at this Reynolds number cannot be explained on the basis of the laminar flow or the bubble flow.

On the other hand, the loci of vanishing turbulent wall shear are affected a great deal by unsteady effects, especially viscous ones, as the hysteresis loops in Fig. 11 show. As discussed in

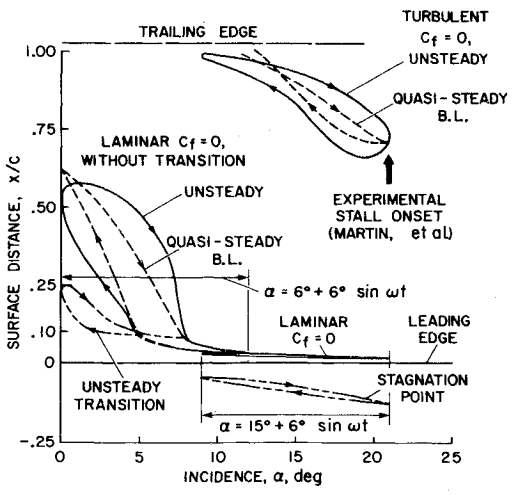

Fig. 11 Dynamic boundary layer characteristics on an NACA 0012 airfoil oscillating at an amplitude of $\pm 6°$. $Re = 3 \times 10^6$, $k = 0.24$.

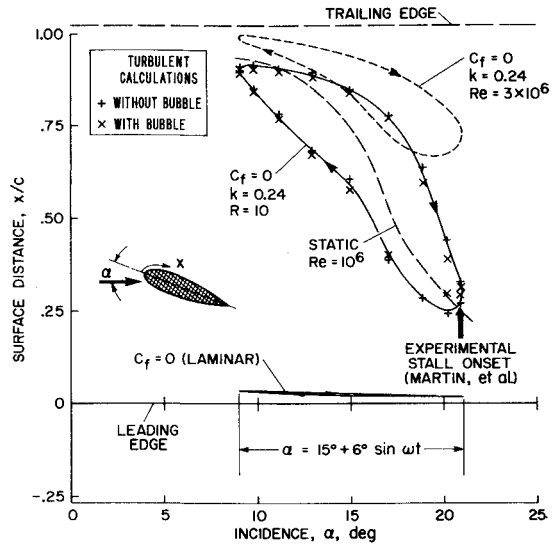

Fig. 12 Effect of Reynolds number on the dynamic boundary layer behavior on an oscillating NACA 0012 airfoil. $\alpha = 15° + 6° \sin \omega t$.

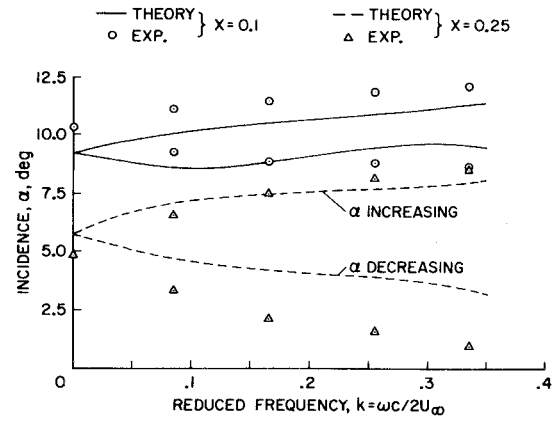

Fig. 14 Effect of reduced frequency on the angle for transition at two points on an airfoil with no stall; $\alpha = 6° + 6° \sin \omega t$, $Re = 0.5 \times 10^6$.

Sec. II, we consider these loci to be intimately related to turbulent separation. The calculated "separation" point moves forward rapidly when the airfoil is near the apex of its motion, and this is the approximate point of stall onset in the experiment.[1] Unfortunately, there is no clue to the formation of the vortex-like disturbance that Martin et al.[1] observed to be shed from the leading edge region.

The effect of Reynolds number on the turbulent separation characteristics is illustrated in Fig. 12. The locus of turbulent $C_f = 0$ moves upstream with decreasing Reynolds number, in both the static and dynamic cases, and the hysteresis loop is considerably larger at $Re = 10^6$. The experimental point[1] of stall onset did not change significantly, however.

In this lower Reynolds number case, the bubble was predicted by Lang's method[16] to burst at $\alpha \approx 11.5°$ on the upstroke, and to reattach at $\alpha \approx 9.5°$ on the downstroke. This compares with the predicted static value of 11.3°, so that some unsteady effects

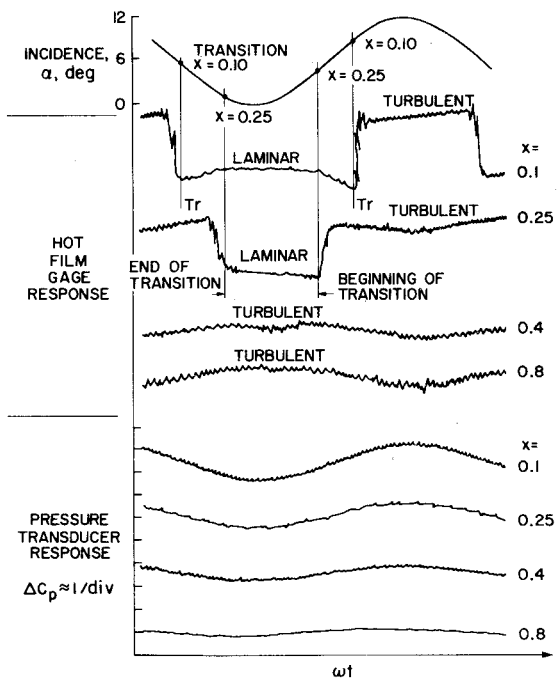

Fig. 13 Representative skin friction and pressure measurements on the ONERA cambered profile; $\alpha = 6° + 6° \sin \omega t$.

are obtained. It should be mentioned that the turbulent calculations are still able to proceed in these cases, because Lang's bursting criterion is only based on the value of the velocity, U_e, at $x_R = x_S + l_1 + l_2$. Lang's value of x_R, as well as Horton's value of θ_R, do not deviate abruptly from the values attained below the bursting angle for these conditions. When these values are used in the manner described previously, the calculated locus of turbulent "separation" is essentially independent of the presence of the bubble.

Oscillating ONERA 0012 Cambré

Figures 7 and 13 show typical responses of the heated film skin friction gages and pressure transducers for the ONERA profile oscillating below stall. Near the leading edge, transition from turbulent to laminar flow and back to turbulent flow again is apparent as the incidence decreases and then increases, and the transition points occur at different angles of attack on the upstroke and on the downstroke due to unsteady effects. The extent and phase of the laminar flow is fairly well predicted by calculations of laminar separation.

Figure 14 shows how varying the reduced frequency changes the angle-of-attack at which points of laminar separation pass over specific gage locations. For the conditions of this example, the incidence always remained well below the stall angle. Theory and experiment show the same tendency for the laminar separation angles at both x-stations to increase with increasing reduced frequency when the airfoil is pitching up, i.e., when $\dot{\alpha} > 0$, although the calculations at $x = 0.10$ are consistently low by about 1°. On the other hand, when $\dot{\alpha} < 0$, the separation bubble moves rearward over the 25% gage location at a slower rate than predicted. In general, the quantitative comparison between theory and experiment is less satisfactory here than the laminar separation results reported in Ref. 3 for the NACA 0012 airfoil. This may be due in part to the sensitivity of the absolute location of the separation points to small changes or imperfections in the airfoil contour.

The case of $\alpha = 9° + 6° \sin \omega t$ portrayed in Fig. 7 is especially interesting, because the maximum incidence is about 1.5° above the static stall angle, and yet the airfoil never stalls in the dynamic case of $k = 0.34$. This provides an unusual test case for the theory. Indeed, quasi-steady calculations predicted separation at the 80% gage location as α approached the maximum value, whereas no separation was predicted at this location when the unsteady effects were included in the calculations.

The final experimental condition to be considered is one which encompasses dynamic stall. Figure 15 shows typical heated film skin friction gage and pressure transducer responses as a function of time, and also the normal force and pitching moment coefficients derived from the pressure measurements. As a result of difficulties encountered with some of the pressure transducers, the curves of C_N and C_M can only be considered qualitative, but

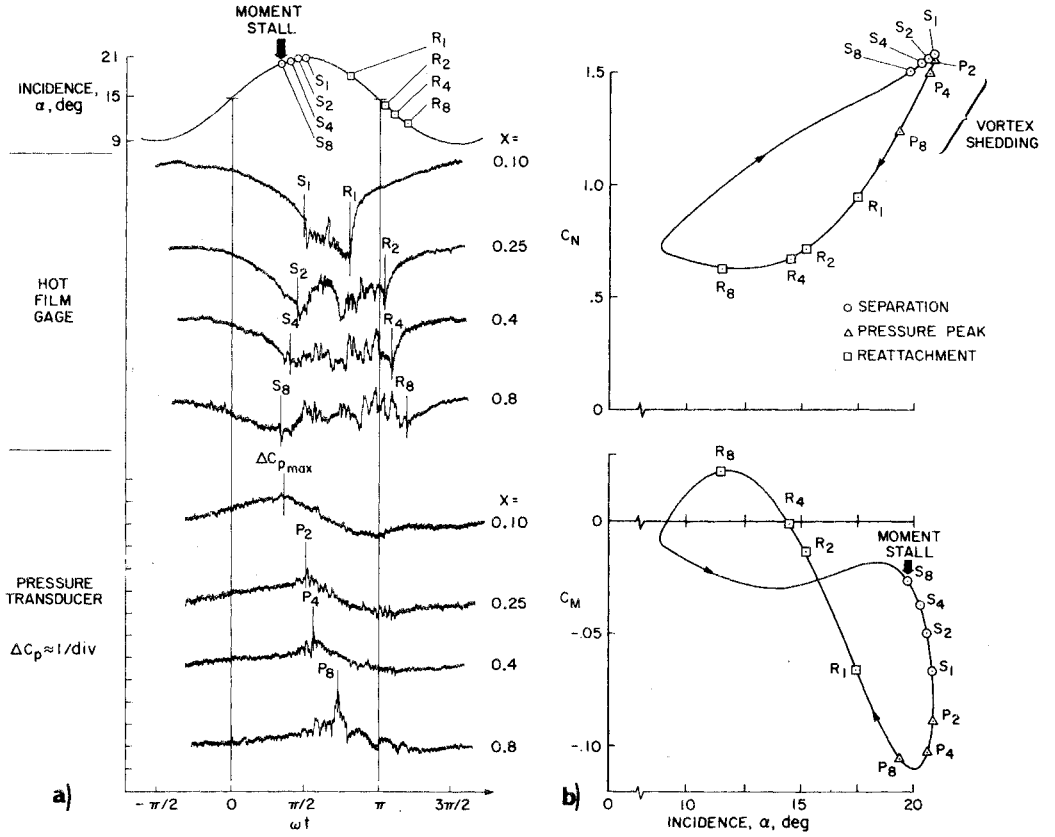

Fig. 15 Representative measurements on the ONERA profile with stall. $\alpha = 15° + 6° \sin \omega t$, $k = 0.152$, $Re = 1.9 \times 10^6$: a) Responses of the pressure transducers and hot film gages; and b) Force and moment coefficients.

large hysteresis effects are apparent nevertheless. The various stall events, e.g., boundary-layer separation, reattachment, and negative pressure peaks due to the passage of the vortex disturbance during stall, are indicated in the figure.

In this case, the measurements indicated a gradual forward progression of turbulent separation as the maximum incidence was approached, complete stall for a brief period, and reattachment of the boundary-layer flow progressing rearward from the leading edge during the downstroke. The suction near the leading edge begins to decrease as soon as the turbulent separation appears at the trailing edge. Just after the separation moves as far forward as $X = 0.10$, a vortex-like disturbance begins to move rearward, inducing a large pressure disturbance similar to the one shown in Fig. 2. The important point here is that whereas Martin et al.[1] were unable to establish the exact sequence of boundary-layer events, here we see clear evidence of a forward movement of trailing edge separation and a distinct effect of this separation on the pitching moment prior to $C_{N_{max}}$. It is interesting to note that the Gault static stall criterion[24] for this airfoil indicates a slightly stronger tendency toward trailing edge stall than the NACA 0012, and this seems to be the trend here.

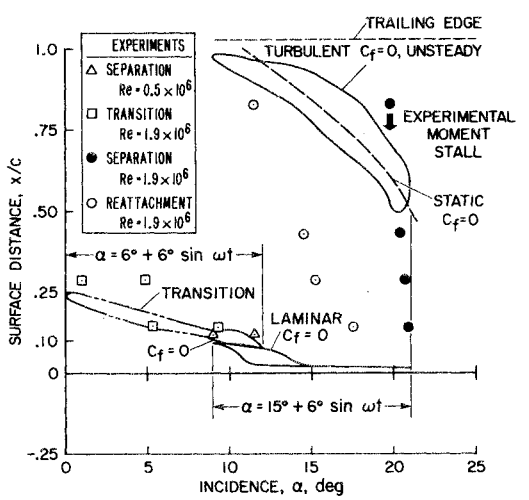

Fig. 16 Dynamic boundary layer characteristics on the ONERA cambered profile oscillating at an amplitude of ±6°. $Re = 1.9 \times 10^6$, $k = 0.152$.

Figure 16 shows the numerical calculations for this case and for a case without stall, in the same format as before. As before, there is no indication of bubble bursting; the bubble only serves to cause transition to turbulence for $\alpha \gtrsim 10°$. At high incidence, the turbulent flow reversal line moves in the general manner as the measured separation and reattachment points, indicative of trailing edge stall. As in the previous cases, the calculated stall onset is less abrupt than indicated by experiment and the measured reattachment process is not well represented by the theory. However, the main shortcoming of the analysis is that there is still no clear indication of the formation and shedding of the vortex-like disturbance that is such an outstanding feature of dynamic stall.

IV. Summary and Conclusions

A combination of analysis and experiment has demonstrated many, but not all, of the essential features of unsteady viscous flow on airfoils and flat plates. The limitations of a classical thin boundary-layer approach, which neglects viscous-inviscid interaction, have been identified. The theoretical model portrayed in the lower half of Fig. 1 seems to provide a valid basis for numerical analysis of airfoil behavior in the absence of dynamic stall, and calculations agree reasonably well with measurements in this case. However, dynamic stall is not well represented.

Calculations show that the impact of unsteady effects on attached laminar flow diminishes rapidly with increasing longi-

tudinal pressure gradients, to the extent of seeming almost negligible insofar as dynamic stall is concerned. On the other hand, unsteady effects seem to become more important with respect to the behavior of the turbulent flow as the incidence of an airfoil increases.

An examination of flat plate flows revealed major and fundamental differences in the structure of unsteady laminar and turbulent boundary layers. In the turbulent case, unsteady effects manifest themselves to a much greater extent in the velocity profiles and displacement thickness than in the wall shear. At high dimensionless frequencies, both eddy viscosity and turbulent kinetic energy formulations of turbulence appear to break down, and in different ways. The turbulent kinetic energy model seems to have a somewhat greater range of validity than the eddy viscosity model, but both are apparently valid for the frequency range of the airfoil cases treated herein.

The main shortcoming of the thin boundary-layer method employed in the present investigation is that it does not provide reliable clues to the formation and shedding of the vortex-like disturbance on an oscillating airfoil, the predominant feature that distinguishes dynamic stall from static stall. This analytical deficiency could arise from one or more of four main areas: 1) an inadequate treatment of the bubble-bursting phenomenon near the leading edge, 2) an incorrect treatment of the turbulent boundary layer immediately downstream of the bubble, 3) an inadequate definition of turbulent separation, especially in unsteady flows, 4) the failure to account for interaction between the boundary layer and the unsteady potential flow around the airfoil. More work needs to be done in each of these areas, and the detailed separation characteristics of the NACA 0012 airfoil especially needs to be documented more completely.

Although we have gained new insight into the fundamental nature of unsteady boundary layers and dynamic stall, much remains to be learned about this difficult and challenging phenomenon. The authors hope that the results presented in this paper will stimuate new and creative theoretical ideas and experimental research.

References

[1] Martin, J. M., Empey, R. W., McCroskey, W. J., and Caradonna, F. X., "An Experimental Analysis of Dynamic Stall on an Oscillating Airfoil," *Journal of the American Helicopter Society*, Vol. 19, No. 1, Jan. 1974, pp. 26–32.

[2] Philippe, J. J. and Sagner, M., "Calcul et Mesure des Forces Aérodynamiques sur un Profil Oscillant, avec et sans Décrochage," *AGARD Conference Proceedings No. 111 on Aerodynamics of Rotary Wings*, Paper 11, Sept. 1972.

[3] McCroskey, W. J., "Recent Developments in Rotor Blade Stall," *AGARD Conference Proceedings No. 111 on Aerodynamics of Rotary Wings*, Paper 15, Sept. 1972.

[4] Ham, N. D. and Garelick, M. S., "Dynamic Stall Considerations in Helicopter Rotors," *Journal of the American Helicopter Society*, Vol. 13, No. 2, April 1968, pp. 49–55.

[5] Crimi, P. and Reeves, B. L., "A Method for Analyzing Dynamic Stall," CR-2009, May 1972, NASA; also AIAA Paper 72-73, San Diego, Calif., 1972; also AGARDograph 172, Nov. 1973.

[6] McCroskey, W. J., "Inviscid Flow Field of an Oscillating Airfoil," *AIAA Journal*, Vol. 11, No. 8, Aug. 1973, pp. 1130–1137.

[7] Theodorsen, T., "General Theory of Aerodynamic Instability and the Mechanism of Flutter," Rept. 496, 1935, NACA.

[8] Bennett, J. A., "Methods of Analysis of Two-Dimensional Airfoils," Rept. ER 8591, Dec. 1966, Lockheed Georgia Co., Marietta, Ga.

[9] Hairston, D. E., "Survey and Evaluation of Current Boundary Layer Transition Prediction Techniques," AIAA Paper 71-985, Washington, D.C., 1971.

[10] Michel, R., "Determination of Transition Point and Calculation of Drag of Wing Sections in Incompressible Flow," ONERA Publication 58, 1952.

[11] Cebeci, T., Smith, A. M. O. and Mosinskis, G., "Calculation of Compressible Adiabatic Turbulent Boundary Layers," *AIAA Journal*, Vol. 8, No. 11, Nov. 1970, pp. 1974–1982.

[12] Shamroth, S. J. and McDonald, H., "An Analysis of the Unsteady Compressible Boundary Layer," *Project SQUID Symposium on Fluid Dynamics of Unsteady, Three-Dimensional and Separated Flows*, 1971.

[13] Sears, W. R. and Telionis, D. P., "Unsteady Boundary Layer Separation," *IUTAM Symposium on Unsteady Boundary Layers*, Quebec, 1971.

[14] Horton, H. P., "A Semi-Empirical Theory for the Growth and Bursting of Laminar Separation Bubbles," Current Paper 1073, 1969, Aeronautical Research Council, England.

[15] Vincent de Paul, M., "Prévision du Décrochage d'un Profil d'Aile en Ecoulement Incompressible," *AGARD Conference Proceedings 102 on Fluid Dynamics of Aircraft Stalling*, Paper 5, 1972.

[16] Lang, J. D., "On Predicting Leading-Edge Bubble Bursting on an Airfoil in Unsteady Incompressible Flow," Memo 109, 1973, Cranfield Inst. of Technology, England.

[17] Roberts, W. B., "A Study of the Effect of Reynolds Number and Laminar Separation Bubbles on the Flow through Axial Compressor Cascades," Ph.D. thesis, Institut d'Aérodynamique, Université Libre de Bruxelles and von Kármán Institute for Fluid Dynamics, 1973.

[18] Gregory, N. and O'Reilly, C. L., "Low-Speed Aerodynamic Characteristics of NACA 0012 Airfoil Section, Including the Effects of Upper-Surface Roughness Simulating Hoar Frost," Aero Rept. 1308, 1970, National Physical Laboratory, England.

[19] Gregory, N., Quincey, V. G., O'Reilly, C. L., and Hall, D. J., "Progress Report on Observation of Three-Dimensional Flow Patterns Obtained during Stall Development on Aerofoils, and on the Problem of Measuring Two-Dimensional Characteristics," Aero Rept. 1309, 1970, National Physical Laboratory, England.

[20] Poisson-Quinton, Ph. and de Sievers, A., "Etude Aérodynamique d'un Elément de Pale d'Hélicoptère," *AGARD Conference Proceedings 22 on Fluid Dynamics of Rotor and Fan Supported Aircraft at Subsonic Speeds*, Paper 4, Sept. 1967.

[21] Abbott, I. H. and von Doenhoff, A. E., *Theory of Wing Sections*, Dover, New York, 1959, p. 462.

[22] Loftin, L. K., Jr. and Smith, H. A., "Aerodynamic Characteristics of 15 NACA Airfoil Sections at 7 Reynolds Numbers from 0.7×10^6 to 9.0×10^6," TN 1945, Oct. 1949, NACA.

[23] Critzos, C. C., Heyson, H. H. M., and Boswinkle, R. W., Jr., "Aerodynamic Characteristics of NACA 0012 Airfoil Section at Angles of Attack from 0° to 180°," TN 3361, Jan. 1955, NACA.

[24] Gault, D. E., "A Correlation of Low Speed Airfoil Section Stalling Characteristics with Reynolds Number and Airfoil Geometry," TN 3963, 1956, NACA.

[25] Dwyer, H. A., "Calculation of Unsteady and Three-Dimensional Boundary Layer Flows," *AIAA Journal*, Vol. 11, No. 6, June 1973; pp. 773–774.

[26] Dwyer, H. A., Doss, E. D., and Goldman, A. L., "A Computer Program for the Calculation of Laminar and Turbulent Boundary Layer Flows," CR 114366, 1970, NASA.

[27] Ames, W. F., *Nonlinear Partial Differential Equations in Engineering*, Academic Press, New York, 1965, pp. 338–357.

[28] McCroskey, W. J., and Durbin, E. J., "Flow Angle and Shear Stress Measurements Using Heated Films and Wires," *ASME Transactions: Journal of Basic Engineering*, Vol. 94, No. 1, March 1972, pp. 46–52.

[29] Lighthill, M. J., "The Response of Laminar Skin Friction and Heat Transfer to Fluctuations in the Stream Velocity," *Proceedings of the Royal Society*, Ser. A, Vol. 224, June 1954, pp. 1–23.

[30] Hill, P. G. and Stenning, A. H., "Laminar Boundary Layers in Oscillatory Flow," *ASME Transactions: Journal of Basic Engineering*, Vol. 82, Sept. 1960, pp. 593–607.

[31] Karlsson, S. K. F., "An Unsteady Turbulent Boundary Layer," *Journal of Fluid Mechanics*, Vol. 5, Pt. 4, May 1959, pp. 622–636.

[32] Schlichting, H., *Boundary Layer Theory*, 6th ed., McGraw-Hill, New York, 1968, pp. 599–600.

[33] Singleton, R. E. and Nash, J. F., "Method for Calculating Unsteady Turbulent Boundary Layers in Two- and Three-Dimensional Flows," *AIAA Journal*, Vol. 12, No. 5, May 1974, pp. 590–595; also NASA TMX-62, 242, Feb. 1973.

[34] Wallis, R. A., "Boundary Layer Transition at the Leading Edge of Thin Wings and Its Effect on General Nose Separation," *Advances in Aeronautical Sciences*, Vol. 3, Pergamon Press, New York, 1962, pp. 161–184.